ISSN 2070-0482, Mathematical Models and Computer Simulations, 2017, Vol. 9, No. 5, pp. 561–569. © Pleiades Publishing, Ltd., 2017.
Original Russian Text © V.D. Ustinov, 2017, published in Matematicheskoe Modelirovanie, 2017, Vol. 29, No. 3, pp. 51–62.

On Inverse Reconstruction Problems of the Erythrocyte Size Distribution in Laser Diffractometry

V. D. Ustinov

Faculty of Computational Mathematics and Cybernetics and the International Laser Center, Moscow State University, Moscow, Russia

e-mail: vladustinov90@gmail.com

Received March 22, 2016

Abstract—The inverse problems of reconstructing the erythrocyte size distribution when the laser diffractometry data is given for the two erythrocyte geometric models—the flat and biconcave disks—are analyzed. It has turned out that when using each of the models the Tikhonov regularization method taking into account a priori information about the smoothness, finiteness, and the nonnegativity of the solution leads to a correct reconstruction of the unknown size distributions for the cases of normal blood, microcytoses, and macrocytoses, characterized by the presence of the factions' abnormally small and abnormally large cells. In the case when the inverse problem is solved on the assumption of a flat particle shape, and the diffraction pattern is calculated by the biconcave disk model, the error in the determination of the first three statistical moments are directly proportional to the magnitude of the deepening in the form of a biconcave disk that simulates erythrocytes. In this case the solution qualitatively coincides with the true distribution, but is shifted relatively to it along the horizontal axis, which in principle can be compensated on the basis of a priori information about the average value of the erythrocyte size distribution.

Keywords: inverse problem, laser diffractometry, erythrocyte, integral equation of the first kind, Tikhonov regularization method

DOI: 10.1134/S2070048217050131

INTRODUCTION

The human red blood cell—an erythrocyte—transports oxygen to the tissues and organs, thus supporting the functioning of the organism as a whole. The recognition of the importance of the erythrocyte size distribution in clinical practice is widespread. The measurement of this distribution width is the standard blood test. It is especially important to measure the cell size distribution in the case of socially significant diseases such as iron deficiency, sickle cell and other blood anemia, spherocytosis, and èlliptocytosis [1]. Several fundamentally different devices are used to measure the size of red blood cells [1] and relatively recently, it was proposed to use a laser diffractometry of blood smears [2] as a potentially fast and reliable method, which allows quickly analyzing the sizes of millions cells, which are simultaneously illuminated by a laser beam.

In this paper the laser light scattering on erythrocytes in the far diffraction zone is considered and the impact of the choice of the cell model on the solution of the inverse problem of reconstructing the cell size distribution according to the small-angle intensity distribution of the scattered light—a diffraction pattern—is analyzed. This theoretical study will specify the operation of a number of devices—laser diffractometers—for measuring the cell distribution by size [2, 3]. In many works the anomalous diffraction approximation is used to describe light scattering on a single cell [2–7], leading to a simple analytical formula for the description of a diffraction pattern. This model implies that the particle shape is a flat disk of a finite small thickness perpendicular to the incident wave. At the same time significantly more complex models are known [8, 9], which allow calculating light scattering by a biconcave disk, representing an erythrocyte in normal conditions. A considerable number of works have been published on the restoring the size distribution of various particle types from the diffraction pattern measured in an experiment. However, the majority of these particles are fundamentally different from erythrocytes in shape, position in space, etc. The application of general methods for the narrowly specialized task discussed in this article can lead to significant errors (see, e.g., [10]), which makes it impossible to apply them to this problem.

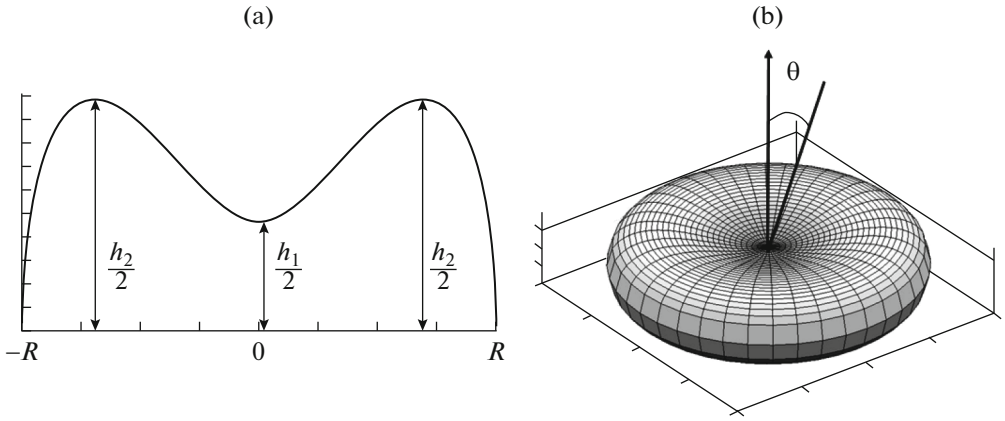

Fig. 1. (a) Skalak curve, rotation of which relative to vertical axis is obtained: (b) biconcave disk of erythrocyte.

Thus, the actual goal of this study is to determine whether the simplification of the geometric model affects the solution of the inverse problem on restoring the erythrocyte size distribution.

1. COMPARISON OF MODELS FOR THE SOLUTION OF THE DIRECT PROBLEM OF LIGHT SCATTERING BY A MONOLAYER OF AN ERYTHROCYTE

Let the laser beam pass through a monolayer of cells located in a thin blood layer between the slides and cover glass, i.e., using a native blood product. The size of one erythrocyte is about 7.5 μm, which is about one order larger than the wavelength of the visible light spectrum; thus, the laser beam is scattered by the erythrocyte predominantly forward, i.e., in the region of the angles, that are small relative to the direction of the propagation of the incident electromagnetic wave. In this case a diffraction pattern occurs in the far zone—the angular intensity distribution of the light scattered forward.

A single erythrocyte is a homogeneous biconcave disc with a relatively constant refractive index $m = 1.05$. This form can be modeled with the Skalak curve [11], where the magnitudes h_1 and h_2 specify the minimum and maximum thicknesses of a red blood cell, respectively (Fig. 1).

From Maxwell's system of equations for the region D_1 inside an erythrocyte with a constant wavenumber k_1 and the region D_2 outside of the erythrocyte with a constant wavenumber k_2 volume integral equation can be derived (see for example [12]):

$$E(M_0) + \int_{D_1} (k_2^2 - k_1^2) G(M, M_0) E(M) dV_M = E^0(M_0), \quad M_0 \in D_1, \tag{1.1}$$

where the vector E is the full field, i.e., the sum of the field of the light scattered by an erythrocyte and the field of the incident wave $E^0(M_0)$, which would be at a given point in the absence of the scattering body D_1, and $G(M, M_0)$ is a 3×3 matrix of Green's functions for homogeneous and piecewise-smooth media. Equation (1.1) is a vector equation and actually contains three scalar integral Fredholm equations of the second kind with singular kernels.

Equation (1.1) is reduced to the system of linear algebraic equations (SLAEs) with a large number of unknowns and allows calculating the light scattering in all the observation angles. In the present work, the ADDA program has been used for the calculations according to this method [9]. The diffraction patterns corresponding to the biconcave disks were obtained using this program. This method is known as discrete-dipole approximation (DDA). It is computationally complex, but allows an arbitrary geometry of a particle.

As in typical laser diffractometry experimental conditions, the light scattering by an erythrocyte is only measured at small angles up to a maximum of 25 degrees relative to the direction of the incident wave, the vector formulation of the problem is reduced to a scalar one due to the fact that the small-angle scattering of light does not depend on the wave's polarization vector. When replacing the true form of an erythrocyte

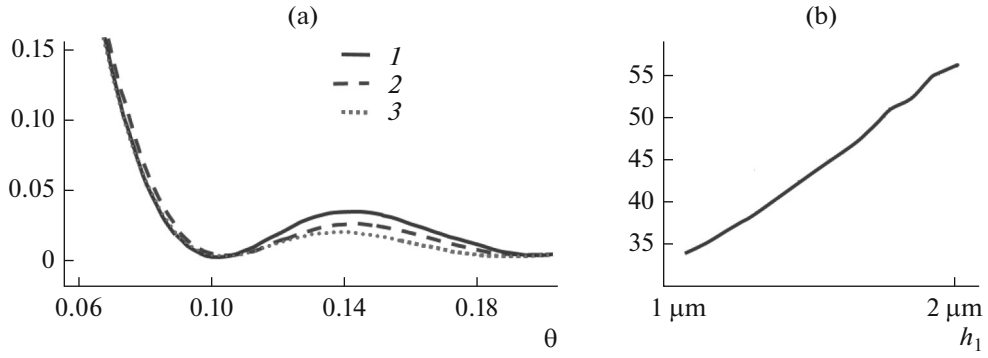

Fig. 2. (a) Dependence of diffraction pattern on scattering angles θ for $h_2 = 2$ μm and $h_1 = 1, 1.5, 2$ (curves *1*, *2*, *3*, respectively); (b) dependence of ratio of central and first local maxima on h_1.

on a flat volume disk of a finitely small thickness h, the approximation of the anomalous diffraction is used [13, 7] to calculate the field intensity of the light scattered by the erythrocyte:

$$|E|^2 = I_1(\theta, R) = L \cdot K(h) \cdot \left(R \frac{J_1(k\theta R)}{\theta} \right)^2, \tag{1.2}$$

where J_1 is the Bessel function of the first kind of the first order and R is the radius of a flat disk with thickness h. The value $K(h) = |1 - \exp(ikh(m-1) \cdot n_0)|^2$, using Shifrin's terminology [7], will be called the erythrocyte weakening diameter, $n_0 = 1.33$ is the refractive index of the medium, L is a dimensional constant that does not depend on R and θ, $k = 2\pi/\lambda$ is the wave number of the incident wave in a vacuum, m is the relative refractive index of the erythrocyte, and λ is the length of the incident wave in a vacuum.

Compare the calculations of the diffraction patterns made using the models of flat and biconcave discs (see further Fig. 2). The peculiarity of the problem is such [13] that if the value of the radius of the erythrocyte is fixed, then for both models the positions of the local minima and maxima of the angular distribution of the light scattering intensity no longer depend on the thicknesses h_1, h_2, and h. Accordingly, the radii in the two models are assumed to be equal, $R = 3.75$ μm, and the values of $h_2 = 2$ μm and $h = (h_1 + h_2)/2$ will be used as physiological values for erythrocytes in the norm, when the value h_1 ranges from 1 to 2 μm.

The fact that at $h_1 = h_2$ a biconcave disk turns into a rounded washer most closely corresponding to the flat disk model was used for calibrating the flat disk model relative to the biconcave disk model. In this case, the diffraction pattern calculation using the ADDA program and in the anomalous diffraction approximation (1.2) showed a good match of the ratios of the central and the first local maximums of the diffraction patterns in each approximation, which characterizes the closeness of the models. For comparison, it can be noted (Fig. 2b) that with h_1 decreasing from 2 to 1 μm this ratio changes by a factor of more than 1.5.

The comparison of the normalized to the central maximum (at $\theta = 0$) diffraction patterns at various h_1 values shows (Fig. 2a) that at the angles θ close to zero (up to the first local minimum), the diffraction patterns for a biconcave and flat disk are close to each other, the influence of the thicknesses h_1, h_2, and h is here very low. However, such small angles are not enough to solve the inverse problem (see, e.g., [10]). Currently the diffraction pattern over a wide range is fairly easily accessible for measurement. At these angles, as seen in Fig. 2a, the difference between the two models are significant, and the influence of which of these magnitudes—h_1, h_2, or h—is chosen is great. However, the diffraction pattern itself in this region also depends on the erythrocyte size in the ensemble, which improves the work of the inverse problem solver. In the next section, we study how the difference between h_1 and h_2 affects the work of the inverse problem solver.

2. THE INVERSE PROBLEM OF DETERMINING THE ERYTHROCYTE SIZE DISTRIBUTION FROM AN ACCURATELY MEASURED DIFFRACTION PATTERN

This section discusses inverse problems in which the target is the erythrocyte size distribution and the well-known inaccurately measured data are the diffraction pattern. Each of these inverse problems is described by Fredholm's scalar integral equation of the first kind:

$$A\omega = \int_{R_1}^{R_2} I(R,\theta)\,\omega(R) = \tilde{I}(\theta), \tag{2.1}$$

where $I(R,\theta)$ is the intensity of the light scattered in direction θ on an erythrocyte with radius R, $\omega(R)$ is the required cell size distribution, $\tilde{I}(\theta)$ is the diffraction pattern measured in the experiment, R_1 is the minimum radius of the erythrocytes in the ensemble, and R_2 is the maximum radius of the erythrocytes in the ensemble. Based on the physiological dimensions of the erythrocytes, we took $R_1 = 2$ μm and $R_2 = 7$ μm.

A detailed derivation of Eq. (2.1) is proposed, for example, in [13]. The important physical conditions for the correct application of Eq. (2.1) are also given there, in particular a single light scattering by the cells and their random arrangement in a fixed plane in the incident wave field.

The difference between the three tasks considered later is in using different kernels $I(R,\theta)$ that meet the choice of the erythrocyte's model geometry. For each of the three tasks, A will be considered as an operator acting from the Sobolev space $W_2^1[R_1, R_2]$ to the Lebesgue space $L_2[0,\theta_{\max}]$, thereby assuming a priori the appropriate smoothness of the physically meaningful erythrocyte distribution. Here and below $\theta_{\max}$ is the maximum viewing angle in radians.

In inverse problem 1, the kernel has form (1.2): $I(R,\theta) = I_1(\theta, R)$, where the cylinder's thickness is $h = (h_1 + h_2)/2$. The corresponding integral operator in the left part (2.1) is denoted by A_1, $\tilde{I}_1$ is the exact right part, $\tilde{I}_{1\delta}$ is the right part measured with the error $\delta_1 = \left\|\tilde{I}_1 - \tilde{I}_{1\delta}\right\|_{L_2[0,\theta_{\max}]}$, and the operator error is assumed to be zero.

In the inverse problem 2, the kernel $I(R,\theta) = I_2(\theta, R)$ is calculated via the solution of the vector integral equation (1.1) for a single erythrocyte. The corresponding integral operator in (2.1) will be denoted by A_2, $\tilde{I}_2$ is the exact right part, $\tilde{I}_{2\delta}$ is the right part with the measurement error $\delta_2 = \left\|\tilde{I}_2 - \tilde{I}_{2\delta}\right\|_{L_2[0,\theta_{\max}]}$, and the operator error is assumed to be zero.

In the inverse problem 3, the right part for the sought distribution $\omega(R)$ is calculated by numerically integrating the left part of (2.1) with the kernel $I_2(\theta, R)$ based on the vector model (1.1); however, the integral equation (2.1) is then solved for a simpler kernel $I_1(\theta, R)$ of the anomalous diffraction (1.2). Such an inverse problem corresponds to the situation often encountered in the literature [2–7] when using a simplified model of a flat disk. However, the data from the field experiment is naturally much closer to the inverse problem 2, as the erythrocyte's physiological form under the normal conditions is biconcave, and not a flat disk. In fact, we can interpret the integral operator with the kernel from problem 1 as specified inaccurately compared to the kernel from problem 2. Then the integral operator in problem 3 has the form $I_2(\theta, R)$, $\tilde{I}_3 = \tilde{I}_2$ is the exact right part, $\tilde{I}_{3\delta} = \tilde{I}_{2\delta}$ is the right part with the measurement error $\delta_3 = \left\|\tilde{I}_3 - \tilde{I}_{3\delta}\right\|_{L_2[0,\theta_{\max}]} = \delta_2$, and the operator error $h_3 = \left\|A_2 - A_1\right\|_{W_2^1 \to L_2}$ is equal to the norm of the bounded linear operators from $W_2^1[R_1, R_2]$ to $L_2[0,\theta_{\max}]$.

The introduced inverse problems are reduced to the solution of integral equations $A_i\omega = \tilde{I}_{i\delta}$, $i = 1,2,3$. It is easy to see that for all three equations the integral operators have continuous kernels. Therefore, the corresponding linear integral operators A_1, A_2, and A_3 are completely continuous from $W_2^1[R_1, R_2]$ to $L_2[0,\theta_{\max}]$. In addition, note that the injectivity of the operator A_1 and $A_3 = A_1$ follows from the results of [15, 16], where the integral operators were considered on a half-line with the kernels of a special form $K(x, t) = K(t \cdot x)$, where $\int_0^\infty |K(s)| \cdot s^{-1/2} ds < \infty$, and the injectivity of the operator A_2 with the kernel of a general form is further assumed a priori. Hence, the integral operators A_i, $i = 1,2,3$ are invertible, $\tilde{\omega}_i = A_i^{-1}\tilde{I}_i$; however, the inverse operators A_i^{-1} are unlimited (see, e.g., [14], s. 20.6).

Thus, the inversion of the integral operator A_i for any of the three inverse problems is unstable for the space of the solutions $W_2^1[R_1, R_2]$ and the space of the right sides $L_2[0, \theta_{\max}]$. This leads to the fact that even the analytical formulas found for the A_1 inversion based on the Mellin integral transformation (see, e.g., [15]), in the case of the right part defined inaccurately (2.1) lead to physically meaningless solutions. Therefore, the regularization according to Tikhonov was used for the numerical treatment of (2.1).

The inverse problems 1, 2, and 3 were solved by reduction to the problem of minimizing the Tikhonov functional with the choice of the regularization parameter by the generalized discrepancy principle. The approximation A_i with accuracy h in the operator norm is denoted as A_{ih}. Consider the Tikhonov functional $M_i^\alpha(\omega) = \left\|A_{ih}\omega - \tilde{I}_{i\delta}\right\|^2_{L_2[0,\theta_{\max}]} + \alpha\|\omega\|^2_{W_2^1[R_1,R_2]}$, where $\alpha > 0$ is the regularization parameter. Following the physical considerations, the set of constraints is defined,

$$\Omega = \left\{\omega(R) \in W_2^1[R_1, R_2]: \ \omega(R_1) = \omega(R_2) = 0, \ \ \omega(R) \geq 0 \ \forall \ R \in [R_1, R_2]\right\},$$

which is closed (theorem on traces in $W_2^1[R_1, R_2]$), convex, and $0 \in \Omega$. Since the Tikhonov functional is strongly convex, a unique extremal $\omega_{i\eta}^\alpha$ exists, leading to the functional minimum:

$$M_i^\alpha(\omega_{i\eta}^\alpha) = \inf_{\omega\in\Omega} M_i^\alpha(\omega), \tag{2.2}$$

where $\eta = (h, \delta)$ is the vector of errors for the operator and the right-hand side of the statement. Consider a discrepancy $\rho_\eta(\alpha) = \left\|A_{ih}\omega_{i\eta}^\alpha - \tilde{I}_{i\delta}\right\|^2_{L_2[0,\theta_{\max}]} - \left(\delta + h\left\|\omega_{i\eta}^\alpha\right\|_{W_2^1[R_1,R_2]}\right)^2$. The choice of the regularization parameter by the generalized discrepancy principle [17, p. 15] consists of the fact that if $\left\|\tilde{I}_{i\delta}\right\|_{L_2[0,\theta_{\max}]} \leq \delta$ then $\omega_{i\eta} = 0$ is taken as an approximate solution of (2.1). If $\left\|\tilde{I}_{i\delta}\right\|_{L_2[0,\theta_{\max}]} > \delta$, then in the case of the existence of $\alpha(\eta)$ such that $\rho_\eta(\alpha(\eta)) = 0$, $\omega_{i\eta} = \omega_{i\eta}^{\alpha(\eta)}$ is assumed, and in the case of $\rho_\eta(\alpha) > 0$ for all $\alpha > 0$ $\omega_{i\eta} = \lim_{\alpha\to+0} \omega_{i\eta}^{\alpha(\eta)}$ is taken. The following statement which is a reformulation of theorem 3 from [17] is true for the considered inverse problems.

Theorem. *If* $\left\|A_{ih} - A_i\right\|_{W_2^1\to L_2} \leq h$, $\left\|\tilde{I}_{i\delta} - \tilde{I}_i\right\|_{L_2[0,\theta_{\max}]} \leq \delta$ then choosing the regularization parameter by the generalized discrepancy principle, at $\eta = (h, \delta) \to 0$, we have $\omega_{i\eta} \to \tilde{\omega}_i$ in the norm of the space $W_2^1[R_1, R_2]$, $i = 1, 2, 3$.

In the computational experiments on the solutions of the inverse problems 1—3, the operators A_i in the left part of (2.1) were replaced by their finite-dimensional analogs (matrices) A_{ih} using the approximation of integrals by partial sums based on the Gauss quadrature with N summands. As the accuracy of the integrals' calculation directly depends on the choice of a sufficiently large N, then, given the characteristic laser diffractometry range of measurement error levels in the diffraction pattern from 1 to 15%, the corresponding evaluation error of the operators in the formula of the residuals was not considered at $i = 1, 2$, and at $i = 3$ it was taken into account with the help of the ratios $\left\|A_{2h} - A_{1h}\right\|_{W_2^1\to L_2} \leq \left\|A_{2h} - A_{1h}\right\|_{L_2\to L_2} = h_3$.

The method of gradient projection was used for finding the extremal in problem (2.2) at fixed α

$$\omega_{k+1} = P_\Omega(\omega_k + \beta A_{ih}^T\tilde{I}_{i\delta} - \beta(A_{ih}^T A_{ih} + \alpha H)\omega_k), \ \ k = 0, 1, \ldots,$$

where P_Ω is the projection operator onto the set Ω, $\beta > 0$ is the gradient projection method step, and the matrix $H = E - \Lambda$, which is the difference between the identity matrix and the matrix of the second differential derivative operator, occurs at the norm approximation in $W_2^1[R_1, R_2]$ (see, e.g., [17, Chapter 1, §5]). In this work, the distribution at which the Tikhonov parametric functional reaches its minimum in the entire space and which is the solution of the linear algebraic equation system $(A_{ih}^T A_{ih} + \alpha H)\omega = A_{ih}^T\tilde{I}_{i\delta}$ was taken as a first approximation. The method β step did not depend on the iteration number and was chosen in accordance with the condition $0 < \beta < 2/\lambda_{\max}$, where $\lambda_{\max}$ is the maximum of the eigenvalue of the matrix $A_{ih}^T A_{ih} + \alpha H$ (e.g., see [18]). The iterations of the gradient projection method ended when a sufficiently small relative change of the solution on doubling the number of iterations had been reached.

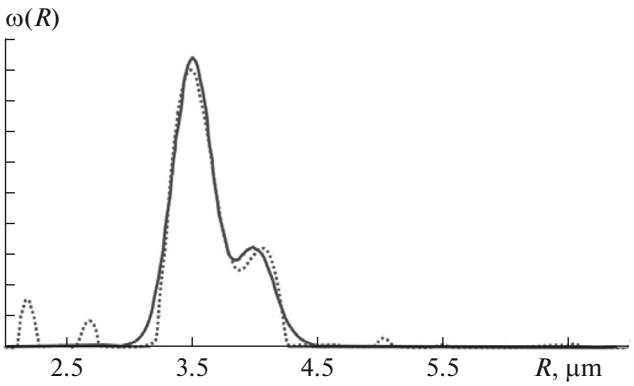

Fig. 3. Example of solving of inverse problem 1 when right side noise level is 15%. Continuous curve denotes predefined bimodal size distribution of erythrocyte. Point curve is working result of inverse problem 1 solver.

The root of the generalized discrepancy was found by the method of the dividing an interval in half. All the numerical calculations were performed using the Matlab Mathworks Software.

Remark on the stability of Eq. (2.1). As mentioned [10], a change of variables $\tilde{\omega}(R) = \omega(R) \cdot R$ significantly improves the stability of the inverse problem solver:

$$\int_{R_1}^{R_2} \left(I(R,\theta) \cdot \frac{\theta^3}{R} \right) \tilde{\omega}(R) dR = \theta^3 \tilde{I}(\theta). \tag{2.3}$$

This replacement makes the dispersion of the kernel values and corresponding SLAEs smaller than the original equation. The influence of the angle $\theta = 0$, which is usually impossible to measure in the experiment, is also eliminated by a replacement. Everywhere further Eq. (2.1) will be solved only using replacement (2.3) with the sought function being subsequently found in the form $\omega(R) = \tilde{\omega}(R)/R$. The task acquires a certain stability starting from the sizes of the wavelength order. The analysis of the singular value decomposition of Eq. (2.3) carried out in [10] shows that the sizes that are smaller than the wavelength weaken the stability of the equation solver. In this regard, the boundary conditions of Dirichlet $\omega(R_1) = \omega(R_2) = 0$ are used in all the algorithms for solving this equation. Given the fact that the wavelength is 0.63 μm, this range lies on the edge of this problem's sustainability and, in fact, has still not been examined. Note that the sustainability depends on the interval width $[R_1, R_2]$ and the interval selection takes into account the a priori information.

3. THE NUMERICAL RESULTS OF THE INVERSE PROBLEM SOLUTION

In this section the numerical results of the solutions of the inverse problems 1–3 described in Section 3 are presented. The two main distributions of erythrocytes in size, corresponding to the medical practice, are considered to illustrate the methods described above:

$$\omega(R) = \exp\{-20 \times (R - 3.5)^2\}, \tag{3.1}$$

$$\omega(R) = \frac{2}{3}\exp\left\{-20 \times (R - 3.5)^2\right\} + \frac{1}{3}\exp\left\{-20 \times (R - 4)^2\right\}. \tag{3.2}$$

Formula (3.1) corresponds to the normal distribution, while (3.2) corresponds to the bimodal distribution, in which there is a 30% fraction of abnormally large cells, in particular, the one directly measured for the case of one of the blood anemias—megacitosis [1]. The determination of the presence and amount of this fraction is of interest. The following interval was selected for the given function: $R_1 = 2$ μm and $R_2 = 7$ μm. Physiologically for a human being the absolute minimum radius is $R_1 = 3$ and the maximum $R_2 = 5$ μm. The interval was selected wider for the computational experiment to make the distribution significantly finite. All the size distribution functions are normalized to the integral $\int_{R_1}^{R_2} \omega(R) dR$; thus, the influence of the unknown number of cells in the ensemble is eliminated.

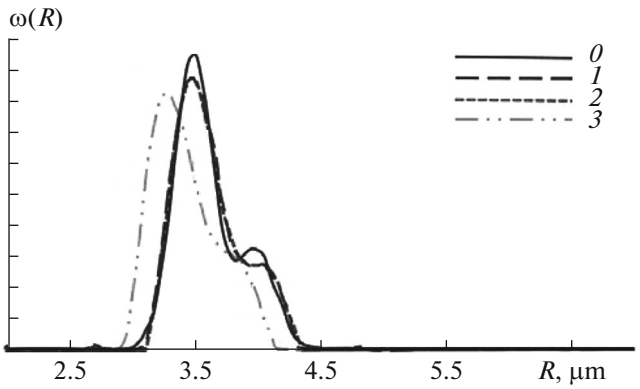

Fig. 4. Sample solution of inverse problems 1–3 (curves *1–3*) with noisy right side (1%) in comparison with exact solution (curve *0*). Number of iterations is 10^4, $h_1/h_2 = 0.5$.

In Fig. 3 the graphs of two functions are shown. The continuous curve denotes a predefined asymmetric bimodal size distribution (3.2), modeling the presence of the normal and abnormally large erythrocyte fractions. The point curve is the result of the inverse problem's numerical solution 1 with a 15% noise level on the right-hand side. Note that the left and right peaks of the size distribution characterizing the normal and abnormally large cells fractions, respectively, were recovered using an accurate numerical solution of the problem. The deviation level of the solution from the true distribution in the small angle region roughly corresponds to the noise level in the right-hand side and, as seen in Fig. 4, almost disappears with the reduction of the noise of the right side to 1%.

In Fig. 4 an example of the solution of the inverse problems 1–3 with the ratio of the erythrocyte thickness in the center to the thickness at the periphery $h_1/h_2 = 0.5$ and with the right side noise level amounting to 1%. In this case the iteration number in the regularization method is 10^4. It is seen that in comparison with the predetermined decision, the solution of problems 1 and 2 restore the location of the main maximum, and the solution of problem 3 is shifted left relative to the true one.

The data for Figs. 3 and 4 were obtained using the desired bimodal distribution. Similar results are also true for the Gaussian distribution (3.1). Many other distributions (trimodal, peak linear, parabola, etc.) were also considered; however, due to the limitation of this article only the cases which are most in demand in applications were presented.

For the application of the diffractometry methods in medical practice, it is important that the average value and the second moment (the distribution width), as well as the approximate third point characterizing the distribution asymmetry, are recovered correctly when solving the inverse problems 1–2. Here and below the nth statistical moment of the distribution is equal to the value of the integral $\int_{R_1}^{R_2} \omega(R) \cdot R^n dR$. The data about the moments make it possible to discover the volume of the abnormally large cell fraction with an accuracy of about 15% at the same noise level. For the bimodal distribution (3.2), the statistical moments of the distribution found by solving problem 3 for different values of h_1/h_2 ranging from a strong bending of the erythrocyte form to the almost complete absence of it at the level of the Gaussian noise of 15% on the right-hand side are presented in Table 1.

Table 1. Problem 3: first three moments for biconcave disk depending on h_1/h_2

First moment	Second moment	Third moment	h_1/h_2
4.90	25.19	134.35	0.40
4.30	19.96	97.68	0.80
3.93	16.30	72.08	0.92
3.70	14.00	54.59	0.99

Table 2. First three moments for problems 1, 2 in comparison with true ones

First moment	Second moment	Third moment	
3.60	13.21	48.42	True
3.60	13.19	49.85	Problem 1
3.63	13.54	41.81	Problem 2

The same data for the solutions of problems 1 and 2, as well as the values of the true distribution moments are presented in Table 2.

It is seen that with a reduction of the depression in the center of the erythrocyte geometric model the values of the first three moments of problem 3 approach the true distribution values. In addition, the error of the restored moments of the size distribution of the erythrocytes for problems 1–2 corresponds to the error of the right-hand side of the equation.

The study of the influence of the choice of the erythrocyte's geometric model on the solution of the inverse problem of laser diffractometry is important from the point of view of finding the size distribution of the erythrocytes under the conditions of a real experiment. In our recent work [19], a field experiment was conducted in which the erythrocyte size distribution, obtained using the solution of Eq. (2.1), was compared with the similar distribution obtained by an alternative method: by using automated optical microscopy. In laser diffractometry the incident wave scatters at the same time on hundreds of thousands of cells, allowing us to use Eq. (2.1) to obtain more accurate information about the fractions of the erythrocytes of different sizes, while the microscopy method typically allows exploring not more than a few thousand cells in the sample. Thus, the models of light scattering by the erythrocytes being developed in this work open the possibility of creating a medical device for the analysis of the size distribution of erythrocytes which will have a number of advantages in comparison with its analogs.

Note that the problem of the additional calibration of the considered models and the compensation of a shift in the position of the main maximum of the recovered distribution identified in the transition to the simplified anomalous diffraction kernel (1.2) is relevant. One of the methods used to solve it is the approximate formula of the dependence between the angular position of the first local minimum of a diffraction pattern and the average value of the size distribution (see, e.g., [3]), allowing evaluating the magnitude of the corresponding distribution shear along the axis OX during the solution of the inverse problem a priori. However, a detailed study of the efficiency of using the a priori information of such type remains a matter for the future.

CONCLUSIONS

The inverse problems of the recovery of the human erythrocyte size distribution with the well-known inaccurate data of the erythrocyte laser diffractometry for two erythrocyte geometric models—flat and biconcave disks—are analyzed in this paper. It turned out that the Tikhonov regularization method, taking into account the a priori information about the smoothness, finiteness, and nonnegativity of the solution, leads to a correct reconstruction of the unknown size distributions for the cases of the norm and the micro- and megacytoses of blood, which are characterized by the presence of factions of abnormally small and abnormally large cells. In the case when the inverse problem is solved assuming the flat shape of a particle and the diffraction pattern is calculated by the model of a biconcave disk, the error in determining the first three statistical moments is directly proportional to the magnitude of the deepening in the form of the biconcave disk that simulates the red blood cells. In this case the solution qualitatively coincides with the true distribution, but is shifted relatively to it along the horizontal axis. Such a behavior of the solution opens the opportunity to correct this error by using a priori information about the average value of the size distribution of an erythrocyte.

ACKNOWLEDGMENTS

This work was supported by the Russian Foundation for Basic Research (grants nos. 13-02-01372, 15-32-51068) and grant UMNICK on the project "Creation of an innovative laser analyzer of red blood cells."

REFERENCES

1. J. D. Bessman and R. K. Johnson, "Erythrocyte volume distribution in normal and abnormal subjects," Blood **46**, 369–379 (1975).
2. Ye Yang, Z. Zhang, X. Yang, J. H. Yeo, L. J. Jiang, and D. Jiang, "Blood cell counting and classification by non-flowing laser light scattering method," J. Biomed. Opt. **9**, 995–1001 (2004).
3. S. Yu. Nikitin, A. E. Lugovtsov, A. V. Priezzhev, and V. D. Ustinov, "Relation between the diffraction pattern visibility and dispersion of particle sizes in an ektacytometer," Quantum Electron. **41**, 843–846 (2011).
4. S. Yu. Nikitin, A. V. Priezzhev, A. E. Lugovtsov, V. D. Ustinov, and A. V. Razgulin, "Laser ektacytometry and evaluation of statistical characteristics of inhomogeneous ensembles of red blood cells," J. Quant. Spectrosc. Rad. Transfer **146**, 365–375 (2014).
5. S. Yu. Nikitin, A. V. Priezzhev, A. E. Lugovtsov, and V. D. Ustinov, "Measuring skewness of red blood cell deformability distribution by laser ektacytometry," Quantum Electron. **44**, 774–778 (2014).
6. J. S. Geert, A. G. Hoekstra and R. M. Heethaar, "Anomalous diffraction by arbitrarily oriented ellipsoids: applications in ektacytometry," Appl. Opt. **33**, 7288–7296 (1994).
7. K. S. Shifrin, *Introduction to Ocean Optics* (Gidrometeoizdat, Leningrad, 1983) [in Russian].
8. A. Doicu, T. Wriedt, and Y. A. Eremin, *Light Scattering by Systems of Particles: Null-Field Method with Discrete Sources: Theory and Programs,* Vol. 124 of *Springer Ser. Opt. Sci.* (Springer, Berlin, Heidelberg, 2006), p. 333.
9. M. A. Yurkin and A. G. Hoekstra, "The discrete-dipole-approximation code ADDA: capabilities and known limitations," J. Quant. Spectrosc. Rad. Transfer **112**, 2234 (2011).
10. J. B. Riley and Y. C. Agrawal, "Sampling and inversion of data in diffraction particle sizing," Appl. Opt. **30**, 4800–4817 (1991).
11. T. Wriedt, J. Hellmers, E. Eremina, and R. Schuh, "Light scattering by single erythrocyte: comparison of different methods," J. Quant. Spectrosc. Rad. Transfer **100**, 444–456 (2006).
12. V. I. Dmitriev and E. V. Zakharov, *Method of Integral Equations in Computational Electrodynamics* (Maks Press, Moscow, 2008) [in Russian].
13. S. Yu. Nikitin, A. V. Priezzhev, and A. E. Lugovtsov, in *Advanced Optical Flow Cytometry: Methods and Disease Diagnoses,* Ed. by V. V. Tuchin (Wiley-VCH, Weinheim, 2011), p. 133.
14. V. A. Trenogin, *Functional Analysis* (Nauka, Moscow, 1980) [in Russian].
15. M. Bertero and E. R. Pike, "Particle size distributions from Fraunhofer diffraction," Opt. Acta **30**, 1043–1049 (1983).
16. J. G. McWhirter and E. R. Pike, "On the numerical inversion of the Laplace transform and similar Fredholm integral equations of the first kind," J. Phys. A: Math. Gen. **11**, 1729–1745 (1978).
17. A. N. Tikhonov, V. V. Stepanov, and A. G. Yagola, *Numerical Methods for Solving Incorrect Problems* (Kluwer Academic, Dordrecht, 1995; Nauka, Moscow, 1990).
18. K. Miller, "Least squares methods for ill-posed problems with a prescribed bound," SIAM J. Math. Anal. **1**, 52–74 (1970).
19. S. Yu. Nikitin, Yu. S. Yurchuk, and V. D. Ustinov, "Laser diffractometry of blood smear and measurement of erythrocyte distribution by size," in *Proceedings of the 6th All-Russia School-Conference with International Participation on Physiology of Circulation, Moscow, Feb. 2–5, 2016* (Maks Press, Moscow, 2016), pp. 117–118.

Translated by N. Petrov